Bull Math Biol (2013) 75:2450–2473
DOI 10.1007/s11538-013-9902-x

Society for Mathematical Biology

ORIGINAL ARTICLE

Cyclic Loading of Growing Tissue in a Bioreactor: Mathematical Model and Asymptotic Analysis

J.V. Pohlmeyer · L.J. Cummings

Received: 21 March 2013 / Accepted: 27 August 2013 / Published online: 24 October 2013

Abstract A simplified 2D mathematical model for tissue growth within a cyclically-loaded tissue engineering scaffold is presented and analyzed. Such cyclic loading has the potential to improve yield and functionality of tissue such as bone and cartilage when grown on a scaffold within a perfusion bioreactor. The cyclic compression affects the flow of the perfused nutrient, leading to flow properties that are inherently unsteady, though periodic, on a timescale short compared with that of tissue proliferation. A two-timescale analysis based on these well-separated timescales is exploited to derive a closed model for the tissue growth on the long timescale of proliferation. Some sample numerical results are given for the final model, and discussed.

Keywords Tissue engineering · Mathematical model

1 Introduction

Tissue engineering is currently a hugely important scientific field, a situation likely to persist for the foreseeable future. It is still a nascent area, but the implications of successful tissue engineering on a large scale are profound. An expanding world population, combined with longer life expectancy over which disease may develop, brings increased demand for replacement tissue (of all types) for transplantation, exacerbating the shortage that already exists (Curtis and Riehle 2001). As a result, doctors and scientists are forced to look for new ways to try to meet the demand. Tissue engineering, with its long-term goals of growing viable tissue or even whole organs artificially, offers promise in this regard. In an ideal scenario, target cells would be harvested from a patient, and used to grow new tissue for later transplant into that

J.V. Pohlmeyer · L.J. Cummings (✉)
Department of Mathematical Sciences, New Jersey Institute of Technology, University Heights, Newark, NJ 07102, USA
e-mail: linda.cummings@njit.edu

same patient. With the patient's own cells used, the risk of rejection should be minimal; however, with tissue growth a relatively slow process, and possibly very sick patients, this approach may not always be practical. Therefore, many other protocols have been and continue to be researched in an effort to determine the best way to obtain functional tissue growth.

One obvious method to determine optimal protocols is to perform many experiments in a lab and see which elicit the best results. However, growing sufficient tissue to validate a given protocol takes days to weeks, so carrying out any kind of parameter study in this way is both expensive and labor-intensive. Building mathematical models of different protocols offers potential to reduce significantly the time needed to obtain and analyze results; an experiment that might take weeks in the laboratory can be simulated in minutes on a computer. A properly calibrated computer model can be used to see how changing parameters or experimental conditions affects the overall outcome, thus (in principle) determining the optimal protocol considerably more efficiently. We review some of the relevant literature in the following, and note that Sengers et al. (2007) compiled a useful review of the multitude of computational models used in tissue engineering, to which the reader is directed for a more comprehensive overview.

A frequently used experimental protocol is to place a cell-seeded porous *scaffold* in a bioreactor filled with nutrient-rich culture medium. The main function of the scaffold is to support the growing tissue as it proliferates. A great deal of research is devoted to scaffold architecture: Pore size and shape (and hence permeability) can be varied, and different biomaterials, with different tensile and compressive strains, may be used. In an early experimental model, Malda et al. (2004) attempted to understand the relationship between local oxygen concentration and the oxygen demand of the cells by measuring the development of oxygen gradients due to cellular oxygen consumption in chondrogenesis. Lewis et al. (2005) went further and examined the interaction between evolving oxygen profiles and cell distributions, formulating a simple mathematical model that they compared to the experiments of Malda et al. (2004).

Both Lewis et al. (2005) and Malda et al. (2004) considered the case in which nutrient is delivered primarily by diffusion (static culture). Lewis et al. (2005) noted that in this case, the result is typically a proliferation-dominated region near the outer edge of the scaffold, with very low cell (and nutrient) concentrations deeper inside the scaffold. To alleviate this problem of "periphery-dominated" scaffolds, nutrient delivery may be enhanced by perfusion (forced flow through the seeded scaffold). In addition to delivering nutrient more efficiently to the scaffold interior, the flow also provides some shear stress, which in some cases may enhance proliferation (this phenomenon of an external mechanical stimulus translating to biochemical activity within the cell—leading here to enhanced proliferation—is known as *mechanotransduction*). To test this, Raimondi et al. (2004) experimentally compared a static culture system, a surface perfused culture system (where nutrient-rich culture media are driven only along surfaces of the scaffold), and a culture system in which nutrient is forced through the whole construct. They found a measurable increase in cell viability when comparing the forced perfusion to the other two methods of nutrient delivery. Additionally, they developed a computational fluid dynamics model to examine

the modulating effect of fluid shear stress on growth, using imaging to obtain details about the scaffold microarchitecture. In a subsequent study, Porter et al. (2005) calculated the fluid shear stress within a three dimensional scaffold, simulating fluid flow within the structure via the Lattice–Boltzmann method (they concluded that the shear stress levels that lead to increased proliferation were actually lower than determined by Raimondi et al. 2004).

These studies, while important, dealt with isolated aspects of the problem and did not attempt to describe the tissue engineered construct in its entirety. Building on this work, more recent models have moved closer to this goal (Chung et al. 2007, 2008; Coletti et al. 2006; O'Dea et al. 2008, 2009; Pohlmeyer et al. 2013; Shakeel et al. 2013). One approach that has met with some success involves treating the different constituent parts as separate domains or phases. Coletti et al. (2006) derived a two-phase model in a three-dimensional perfusion bioreactor and examined the interactions between the changes in scaffold properties (due to cell proliferation) and the nutrient-rich culture medium on a macroscopic scale. In another two-phase model, Shakeel et al. (2013) focused on the effects of different initial cell seeding density and scaffold pore structure, and examined how these differences affected cell proliferation and the resulting tissue structure. Chung et al. (2007) developed a three-layer model of cell proliferation, nutrient uptake, and culture medium circulation within a porous scaffold under perfusion, the scaffold itself being held between two fluid layers.

None of these works deal with the cells explicitly as a separate phase; instead cells are modeled as nutrient sinks, and proliferation is modeled via changing scaffold permeability and porosity. O'Dea et al. (2008) considered the cells as an explicit phase, and considered the effect of mechanotransduction on local cell density. In subsequent work, these authors explicitly accounted for the scaffold and its interactions with the growing cells (O'Dea et al. 2009) in a three-phase model (cell population and attendant ECM, porous scaffold, and culture medium), deriving a simplified model based on an assumption of slender geometry (i.e., a long wavelength analysis). In a direct extension of this work, Osborne et al. (2010) considered a finite element solution of the analogous full (nonslender) system.

Another mechanotransductive system that has received increasing attention in recent years is a cartilage or bone bioreactor within which the construct (scaffold plus cells) undergoes cyclic compression. The rationale behind such mechanical loading is that it mimics the experience of cartilage/bone within a joint *in vivo* and should thus provide an ideal environment. As cartilage is a relatively avascular tissue, it poses a unique engineering challenge: without a defined vasculature, delivery of nutrient to the entire scaffold is much more difficult, and perfusion could be key. Significant experimental and modeling work has been carried out over the last two decades to find the best way to engineer cartilage. Cyclic loading (and the manner in which it is applied) appears to affect a very wide range of experimental outcomes, in ways that are not yet fully understood. For example, Mauck et al. (2000) discovered that different types of scaffolds with differing stiffness and modulus can greatly affect the end result of an experiment under the same dynamic loading; Schätti et al. (2011) investigated how loading affects differentiation of stem cells (derived from bone marrow) into different cell types, and found that only samples which had both shear and strain

stresses applied showed a significant up-regulation of chondrogenic genetic markers; Wang et al. (2013) found that mechanical loading can stimulate GAG synthesis, up-regulate chondrogenic markers and improve matrix accumulation in cell-laden constructs; and Buschmann et al. (1995) observed chondrocytes under static and dynamic loading, and concluded that application of a mechanical load may significantly alter the long-term development of the tissue.

Among the earliest experimental studies of how cyclic compressive loading affects a perfusion bioreactor was the work of El Haj et al. (1990), in which bone biopsies were simultaneously perfused and subjected to mechanical loading. A marked increase in cell viability was observed in the loaded case when compared to the control. This work is reviewed, along with much other relevant experimental work, in a recent review article by El Haj and Cartmell (2010). Regarding the specific effects of pulsatile or oscillatory shear stress due to unsteady perfusion, in another recent review, McCoy and O'Brien (2010) compile a useful table summarizing the results of 45 different experimental studies utilizing a combination of steady and oscillatory shear stress. Interestingly, while the oscillatory/pulsatile shear is invariably associated with a differentiation response (osteogenic in the cases reviewed), only two instances are noted of enhanced proliferation under oscillatory shear.

Modeling and simulation of loading (steady or cyclic) on the tissue engineering construct can potentially provide significant insight into the effects that stress and/or strain plays in chondrocyte proliferation. Some progress has been made in this direction (for example, the finite-element studies of Babalola and Bonassar 2009 and Moo et al. 2012); but a unified macroscopic model, which treats the entire construct under forced perfusion and cyclic loading, is lacking. In the current paper, we take a step toward this goal by modifying an existing model of ours for tissue growth within a nutrient-perfused porous scaffold (Pohlmeyer et al. 2013) to account also for cyclic loading of the scaffold. We consider a two-phase model describing nutrient transport and proliferation of cells (we assume chondrocytes for estimation of model parameters, but the basic model is quite generic and applicable to many cell types) in a porous scaffold perfused with culture medium (see the schematic in Fig. 1). We capture the effect of perfused nutrient-rich flow, governed by Darcy's law, via upstream and downstream boundary conditions on the pressure; both pulsatile and nonpulsatile driving scenarios are considered. Cell density is explicitly modeled in the system and increases as cells take up nutrients from the flow and proliferate. Cells proliferate due to nutrient uptake at a rate modulated by the local fluid shear stress: We assume increased cell proliferation at moderate shear stress and reduced proliferation when shear stress is excessive. As cells proliferate, they fill the scaffold pores, leading to a decrease in scaffold permeability. To mimic the cyclic compression, the permeability is assumed to vary periodically in time. The cells may also move within the scaffold via cellular diffusion in response to overcrowding and a small advective velocity (proportional to the speed of the fluid flow; essentially, a fluid drag on the cells). Although, as noted above, the cyclic loading is known to influence many experimental variables, we focus here on its effect within the constraints of the simple model outlined in this paragraph—that is, its effect via shear fluid stress modification—comparing total cell proliferation at large times with the unloaded case.

The incorporation of cyclic scaffold compression, which necessarily occurs on the same timescale of the fluid flow within the construct, requires a different approach

from that of Pohlmeyer et al. (2013). Crucially, we can no longer assume steady flow and work on the timescale of cellular growth from the outset, as was done in that paper. The flow is oscillatory, and a careful two-timescale analysis is required: The cyclic loading and the fluid pressure vary on a short timescale, driving the flow, while cell proliferation occurs on a much longer timescale. We also assume a scaffold permeability that varies on the fluid-flow timescale, based on the idea that pores shrink periodically under the compression. While nutrient is transported by advection and diffusion within the fluid, with advection dominating, we consider the case in which a constant external fresh supply keeps the construct well nourished. This approximation, justified in more detail in Sect. 4, enables us to average over an arbitrary loading cycle to obtain the long-time evolution of the cells in terms of cycle-averaged flow quantities. Thus, we are able to use a short timescale average of the fluid flow, which removes all short timescale dependence, and see its effects on cell proliferation on the longer timescale.

In broad agreement with the results summarized by McCoy and O'Brien (2010), we find that whether the shear is steady or oscillatory makes little difference to the level of cellular proliferation. In contrast to findings for compression bioreactors summarized by El Haj and Cartmell (2010), however, the compression also makes little difference. This suggests that, while our basic model is fairly robust, additional modeling is needed specifically to incorporate oscillatory-loading driven mechanotransductive effects. Some possible future modeling directions along these lines are briefly considered, but not simulated in detail, in this paper.

The paper is laid out as follows. In Sect. 2, we briefly describe the basic dimensional model, followed by a general nondimensionalization of the model in Sect. 3, where we also present the relevant parameters used in the simulations. In Sect. 4, we present the leading order analysis of the system and see the separation of physical effects into the two distinct timescales. The short timescale period averaging and its effects on the constituent equations are described in Sect. 4.1. We present the more detailed functional forms that complete the model in Sect. 5, and the full model, together with the numerical approach taken, is summarized in Sect. 6. Sample simulation results are presented in Sect. 7. Some possible extensions to the model are outlined in Sect. 8, and we conclude with a discussion in Sect. 9.

2 Model Formulation

We begin by presenting a full dimensional model as derived in Pohlmeyer et al. (2013), in which asterisks denote dimensional quantities. The idealized experimental set-up is sketched in Fig. 1 where the domain on which we solve (the porous scaffold in the sketch) is a square two-dimensional Cartesian grid with $\boldsymbol{x}^* = (x^*, y^*)$ in which culture medium flows from $x^* = 0$ to $x^* = L^*$ with fixed impenetrable walls at $y^* = 0$, $y^* = L^*$. The culture medium flows with velocity $\boldsymbol{u}^*$ according to Darcy's law (velocity proportional to the gradient of the pressure, p^*), where the scaffold permeability $k^*(c^*, t^*)$ is a function of time t^* and $c^*(\boldsymbol{x}^*, t^*)$, the local cell density. We mimic cyclic compression in the scaffold by prescribing a time-periodic variation in the permeability (with implications for periodicity of the fluid flow), the

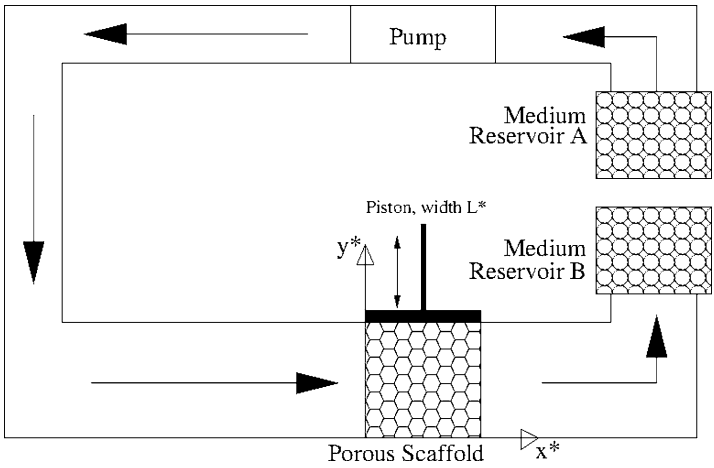

Fig. 1 Schematic of experimental set-up. Fresh nutrient-rich culture medium is pumped at prescribed flow rate from reservoir A, through the porous cell-seeded scaffold, and collected in reservoir B

details of which will be described later. The culture medium, containing nutrient at concentration $n^*(\boldsymbol{x}^*, t^*)$ satisfies an advection-diffusion-reaction equation with advective velocity $\boldsymbol{u}^*$ and an uptake term (sink) due to consumption by the cells. We model the proliferating cell density $c^*(\boldsymbol{x}^*, t^*)$ by considering basic mass conservation principles, incorporating growth (source) terms due to the nutrient consumption (with growth rate dependent on the shear stress, τ_s^*). We also account for cell death, which may in practice be due to several factors (natural death, death due to locally low nutrient concentration, death due to excessively high local shear, etc.). The full dimensional system is

$$\boldsymbol{u}^* = -\frac{k^*(c^*, t^*)}{\mu^*}\nabla^* p^*, \tag{1}$$

$$\nabla^* \cdot \boldsymbol{u}^* = 0, \tag{2}$$

$$\frac{\partial n^*}{\partial t^*} + \boldsymbol{u}^* \cdot \nabla^* n^* = D^* \nabla^{*2} n^* - \theta^* g^*\left(n^*, c^*, \tau_s^*\right), \tag{3}$$

$$\frac{\partial c^*}{\partial t^*} + \boldsymbol{u}_c^* \cdot \nabla^* c^* = D_c^* \nabla^{*2} c^* + \lambda^* g^*\left(n^*, c^*, \tau_s^*\right) - \nu^* c^*, \tag{4}$$

where $g^*(n^*, c^*, \tau_s^*)$ is the nutrient uptake/cell growth term and, along with the permeability k^*, will be discussed in more detail later. The cellular advective velocity, $\boldsymbol{u}_c^*$ is assumed to be due to fluid drag and proportional to the fluid pore velocity $\boldsymbol{u}_p^*$: $\boldsymbol{u}_c^* = \delta \boldsymbol{u}_p^*, \delta \ll 1$; D^* and D_c^* are diffusion coefficients; θ^* is the rate of nutrient uptake; λ^* is the cell proliferation rate; and ν^* is the cell death rate (here assumed constant). Note that the source term in the cell density equation mirrors the sink term in the nutrient equation, reflecting an assumption that proliferation is proportional to the nutrient consumed. This same assumption (though with a much simpler form of g^* than we shall use) appeared in the static culture model of Lewis et al. (2005),

though not in the work of Shakeel et al. (2013). Lewis et al. also neglected any diffusive motion of the cells within the scaffold, so that areas devoid of cells initially would remain so for all time. A more detailed derivation of the model (1)–(4) is given in Pohlmeyer et al. (2013).

3 Nondimensionalization

We wish to model the effects of a periodic compressive force on the scaffold, which, since it drives flow, necessarily occurs on the same timescale as the fluid velocity. Thus, we nondimensionalize the system (1)–(4) as follows:

$$\boldsymbol{x}^* = L^* \boldsymbol{x}, \qquad t^* = \frac{\tilde{t}}{\omega^*} = \frac{T}{\lambda^*}, \tag{5}$$

$$\boldsymbol{u}^* = u_0^* \boldsymbol{u} = L^* \omega^* \boldsymbol{u}, \qquad p^* = \frac{\mu^* L^* u_0^*}{k_s^*} p = \frac{\mu^* L^{*^2} \omega^*}{k_s^*} p, \tag{6}$$

$$n^* = n_0^* n, \qquad c^* = c_0^* c,$$

$$k^*\left(c^*, t^*\right) = k_s^* k(c; \tilde{t}, T), \qquad g^*\left(n^*, c^*, \tau_s^*\right) = c_0^* g(n, c, \tau_s), \tag{7}$$

where $2\pi/\omega^*$ is the period of cyclic loading, $u_0^* = L^*\omega^*$ is the fluid velocity scale, λ^* is the cell proliferation rate, $\tilde{t}$ is the short timescale (on the order of fluid flow) and T is the long timescale (on the order of cell proliferation), μ^* is the fluid viscosity, and k_s^* is the permeability of the unseeded uncompressed scaffold, assumed spatially uniform. We assume (see Table 2) that $\epsilon = \lambda^*/\omega^* \ll 1$.

Nutrient Concentration Dividing Eq. (3) through by $\omega^* n_0^*$ yields the dimensionless form of the nutrient equation

$$\frac{\partial n}{\partial \tilde{t}} + \boldsymbol{u} \cdot \nabla n = D\nabla^2 n - \theta g(n, c, \tau_s), \tag{8}$$

where $D = D^*/(\omega^* L^{*^2})$, and $\theta = (\theta^* c_0^*)/(\omega^* n_0^*)$ with approximate dimensional parameter values defined in Table 1.

Cell Density As with the nutrient equation, we divide the cell density equation (4) through by $\omega^* c_0^*$ to obtain the dimensionless form

$$\frac{\partial c}{\partial \tilde{t}} + \epsilon d \boldsymbol{u}_p \cdot \nabla c = \epsilon D_c \nabla^2 c + \epsilon g(c, n, \tau_s) - \epsilon \nu c, \tag{9}$$

where $\epsilon = \lambda^*/\omega^* \ll 1$, $d = \delta/\epsilon$, $D_c = D_c^*/(\lambda^* L^{*^2})$, $\nu = \nu^*/\lambda^*$, and d, D_c, ν, $g(c, n, \tau_s) \leq \mathcal{O}(1)$ with respect to ϵ (see Table 1). The dimensionless pore velocity is related to the Darcy velocity by $\boldsymbol{u}_p = \boldsymbol{u}/\phi$, where ϕ is the scaffold porosity (related to the permeability k; see Sect. 5 later).

Table 1 Dimensional parameter values (from Shakeel et al. 2013 unless otherwise noted)

Parameter	Name	Value
D^*	Nutrient diffusion coefficient	1.3×10^{-9} m^2/s (Lutianov et al. 2011; Zhou et al. 2004)
L^*	Scaffold length	0.01 m
U^*	Pump flow velocity	5×10^{-4} m^2/s
ω^*	Compression frequency	5 s^{-1}
θ^*	Maximum nutrient consumption rate	4.1667×10^{-18} moles/(cell s) (Lutianov et al. 2011; Zhou et al. 2004)
c_0^*	Representative cell density	10^{15} cells/m^3 (Lutianov et al. 2011)
D_c^*	Cell diffusion coefficient	10^{-13} m^2/s (Obradovic et al. 2000)
λ^*	Cell proliferation timescale	2.315×10^{-6} s^{-1} (Obradovic et al. 2000)
ν^*	Natural cell death rate	3.3×10^{-7} s^{-1}

Table 2 Dimensionless parameter values

Parameter	Formula	Value
D	$D^*/(\omega^* L^{*^2})$	2.6×10^{-6}
θ	$(\theta^* c_0^*)/(\omega^* n_0^*)$	Assumed $\mathcal{O}(\epsilon)$
D_c	$D_c^*/(\lambda^* L^{*2})$	4.32×10^{-4}
ν	ν^*/λ^*	0.1425
ϵ	λ^*/ω^*	4.63×10^{-7}
d	δ/ϵ	10^{-3}

Fluid Flow Finally, the dimensionless forms of Eqs. (1) and (2) are

$$\boldsymbol{u} = -k(c,t)\nabla p, \tag{10}$$

$$\nabla \cdot \boldsymbol{u} = 0. \tag{11}$$

4 Asymptotic Analysis

We seek solutions to Eqs. (8)–(11) as asymptotic expansions in terms of the small parameter ϵ. This is done to exploit the two well-separated timescales to be investigated: the short timescale $t = \tilde{t}$, based on the loading period, and the long timescale $T = \epsilon\tilde{t}$, on which cell proliferation occurs. We assume asymptotic expansions in the form of

$$c(\boldsymbol{x}; t, T) = c_0(\boldsymbol{x}; t, T) + \epsilon c_1(\boldsymbol{x}; t, T) + \cdots, \tag{12}$$

(and similarly for other dependent variables) where all c_i are functions of space and both time variables. Note that, since $t = \tilde{t} = T/\epsilon$, we have

$$\frac{\partial}{\partial \tilde{t}} c(\boldsymbol{x}; t, T) = \frac{\partial c}{\partial t} + \epsilon \frac{\partial c}{\partial T}. \tag{13}$$

Leading Order Nutrient Concentration: Well-Nourished Limit The values estimated in Table 2 suggest that $D = \mathcal{O}(\epsilon)$ and we assume additionally that nutrient concentration in the culture medium is sufficiently high that $\theta = \mathcal{O}(\epsilon)$. In this case, the leading order nutrient concentration equation is just

$$\frac{\partial n_0}{\partial t} + \boldsymbol{u}_0 \cdot \nabla n_0 = 0. \tag{14}$$

If we assume further that the external nutrient supply is held constant, even over the long timescale, then the solution to this equation is just $n_0 = \text{constant} = 1$, with our assumed scaling. This assumption places our model in a different regime to the work of Lewis et al. (2005) and Shakeel et al. (2013) (for example), where lower overall nutrient concentrations lead to results that reflect nutrient depletion zones, concomitant with proliferation suppression.

Leading Order Cell Density Inserting the asymptotic expansion for the cell density, Eq. (12), into the leading order cell density equation (9), and using our two-timescale assumption, we obtain at leading order

$$\frac{\partial c_0}{\partial t} = 0. \tag{15}$$

Thus, we see that the leading order cell density is unchanged on the short timescale, but may vary on the long timescale. At $\mathcal{O}(\epsilon)$ we obtain

$$\frac{\partial c_1}{\partial t} + \frac{\partial c_0}{\partial T} + d\boldsymbol{u}_{p_0} \cdot \nabla c_0 = D_c \nabla^2 c_0 + g(n_0 = 1, c_0, \tau_s) - \nu c_0, \tag{16}$$

where the leading order pore velocity $\boldsymbol{u}_{p_0} = \boldsymbol{u}_0/\phi$, with ϕ the scaffold porosity. We now have one equation with two dependent variables, c_0 and c_1. In Sect. 4.1 we will eliminate c_1 from the equation giving us one equation with one dependent variable.

Leading Order Fluid Flow The fluid flow (Darcy) velocity is obtained by solving an elliptic PDE for the pressure p, which depends on the scaffold permeability

$$\nabla \cdot \big(k(c,t)\nabla p\big) = 0, \quad k(c,t) = (1 + \Delta \cos t)\tilde{k}(c), \tag{17}$$

which we solve subject to no-flux conditions at boundaries $y = 0, 1$ and specified flow conditions at $x = 0, 1$. The form of the permeability used in Eq. (17) contains both spatial and (periodic) temporal dependence; the latter models the effects of the cyclic compression. We have seen that cell proliferation occurs only over the long timescale, so the cell density dependent permeability $\tilde{k}(c)$ is automatically constant over the short time. To simulate the cyclic compression of the scaffold, we have included a 2π-periodic variation on the short timescale $t = \tilde{t}$. Here, $\Delta < 1$ is a coefficient measuring the degree of compression of the scaffold; for this paper, we take $\Delta = 0.2$. With the appropriate asymptotic expansions for cell density and pressure, the leading order Darcy's law and incompressibility equations are

$$\boldsymbol{u}_0 = -(1 + \Delta \cos t)\tilde{k}(c_0)\nabla p_0 \tag{18}$$

$$\nabla \cdot \boldsymbol{u}_0 = 0 \quad \Rightarrow \quad \nabla \cdot \left(\tilde{k}(c_0)\nabla p_0\right) = 0. \tag{19}$$

Since the permeability is 2π-periodic in t, we may assume the leading order velocity $\boldsymbol{u}_0$ and pressure p_0 are also. We consider unidirectional flow driven by a prescribed (dimensionless) flux Q_0. This corresponds to some (unknown) pressure drop Π_0 between $x = 0$ and $x = 1$ across the scaffold. We solve (18) and (19) by exploiting the linearity: Let $\tilde{p}$ be the specific solution of the elliptic PDE (19) satisfying no-flux conditions at $y = 0, 1$ and with a unit pressure drop in x:

$$\tilde{p}(0, y, t) = 1, \qquad \tilde{p}(1, y, t) = 0. \tag{20}$$

Clearly, p_0 and $\tilde{p}$ are related by $p_0 = \Pi_0 \tilde{p}$. The prescribed flux Q_0 satisfies

$$Q_0 = -\int_0^1 (1 + \Delta \cos t)\tilde{k}(c_0)\frac{\partial p_0}{\partial x}\bigg|_{x=0} dy = \Pi_0 \tilde{Q}_0(1 + \Delta \cos t), \tag{21}$$

where $\tilde{Q}_0 = -\int_0^1 \tilde{k}(c_0)\frac{\partial \tilde{p}}{\partial x}|_{x=0} dy$ can be evaluated from the solution $\tilde{p}$. Hence, $\Pi_0 = Q_0/(\tilde{Q}_0(1 + \Delta \cos t))$ from which we recover

$$p_0 = \frac{Q_0 \tilde{p}}{\tilde{Q}_0(1 + \Delta \cos t)}, \tag{22}$$

and thus

$$\boldsymbol{u}_0 = -\frac{Q_0}{\tilde{Q}_0}\tilde{k}(c_0)\nabla \tilde{p}. \tag{23}$$

If the imposed dimensionless flux Q_0 is constant we may set it to 1. Alternatively, we may consider an imposed time-dependent flux $Q_0(t)$ that is also 2π-periodic,

$$Q_0(t) = 1 + A \cos t, \tag{24}$$

for some prescribed amplitude A.

4.1 Period Averaging

We observe that on the short (t) timescale the leading order cell density c_0 is independent of t, as is the nutrient concentration n_0, while the permeability k, porosity ϕ, fluid velocities $\boldsymbol{u}_0$, $\boldsymbol{u}_{p_0}$ and pressure p_0 are 2π-periodic in t. It follows that the shear stress τ_s within the scaffold is also 2π-periodic. Hence, in Eq. (16), the $\mathcal{O}(\epsilon)$ cell density c_1 must also be 2π-periodic. We may therefore average this equation over an arbitrary loading period,

$$\begin{aligned} &\frac{1}{2\pi}\int_{t_0}^{t_0+2\pi}\left(\frac{\partial c_1}{\partial t} + \frac{\partial c_0}{\partial T} + d\boldsymbol{u}_{p_0}\cdot\nabla c_0\right)dt \\ &\quad = \frac{1}{2\pi}\int_{t_0}^{t_0+2\pi}\left(D_c\nabla^2 c_0 + g(n_0 = 1, c_0, \tau_s) - \nu c_0\right)dt, \end{aligned} \tag{25}$$

yielding (using the above observations)

$$\frac{\partial c_0}{\partial T} + d\overline{\boldsymbol{u}_{p_0}} \cdot \nabla c_0 = D_c \nabla^2 c_0 + \overline{g(n_0 = 1, c_0, \tau_s)} - \nu c_0, \tag{26}$$

where the overbars denote the 2π average of the quantity. Given ϕ, the period averaged pore velocity $\overline{\boldsymbol{u}_{p_0}}$ is easily calculated using the results of Sect. 4 above. To calculate $\overline{g(n_0, c_0, \tau_s)}$, we must first define it explicitly.

5 Permeability and Nutrient Uptake Function

To close the model, we propose specific functional forms for the cell density dependent portion of the permeability, $\tilde{k}(c)$, the relation between permeability and porosity ϕ, and the nutrient uptake/cell proliferation function, $g(c, n, \tau_s)$ (see also Pohlmeyer et al. 2013).

Permeability and Porosity As cell density increases, we assume the permeability function will decrease ($\tilde{k}(c) \to 0$ as $c \to \infty$), and as cell density approaches zero, $\tilde{k}(c) \to 1$ due to the nondimensionalization by the permeability of the unseeded unloaded scaffold. Similarly, the scaffold porosity and permeability are also related (though the precise details depend on the scaffold pore geometry), with $k \to 0$ as $\phi \to 0$ and $k \to \infty$ as $\phi \to 1$. Many functional forms satisfy these basic criteria; following Pohlmeyer et al. (2013) we choose

$$\tilde{k}(c) = \frac{1}{1 + c^2} \quad \text{and} \quad k = \frac{\phi^2}{1 - \phi^2} \tag{27}$$

where, recall, $k = (1 + \Delta \cos t)\tilde{k}$.

Nutrient Uptake/Cell Proliferation Function We anticipate that at low cell numbers proliferation will occur at a rate proportional to the cell density, but at high cell numbers overcrowding and competition for resources will lead to saturation. Thus, we choose a logistic model for the dimensionless growth function $g(n, c, \tau_s)$,

$$g(n, c, \tau_s) = G(\tau_s) c \left(1 - \frac{c}{\hat{c}(n)}\right), \tag{28}$$

where $\hat{c}(n)$ is the carrying capacity cell density (which in general depends on nutrient concentration) and $G(\tau_s)$ is the functional dependence on shear stress. In a more sophisticated model, we should specify the functional dependence $\hat{c}(n)$ (see Pohlmeyer et al. 2013) but with $n \equiv 1$ in our model the carrying capacity is constant. Since we assume a well-nourished system, the carrying capacity is more representative of the cells' proliferative response to overcrowding than of the response to the competition for nutrient. We set $\hat{c} = 5$ throughout our simulations, representing a scaffold that is fairly densely seeded initially; a larger value could be used to model a more sparsely seeded scaffold. For brevity, in this publication we do not study the effects of varying this parameter.

Shear Stress Dependence Based on experimental work (by Obradovic et al. 2000), Lappa et al. noted that for moderate shear stress levels, the proliferation rate increases as the square root of shear stress (Lappa 2003). We also want to allow for the detrimental effect of excessive shear, hence we choose

$$G(\tau_s) = \frac{\tau_s^{1/2}}{1+\tau_s}, \tag{29}$$

where the shear stress itself is of the form

$$\tau_s = |\nabla p_0|\sqrt{1+k(c_0)}, \tag{30}$$

with k given by (17) and (27) (this follows from a simple estimate of the velocity gradient within a pore; see Pohlmeyer et al. 2013 for a detailed derivation).

6 Model Summary and Numerical Approach

We solve for the leading order cell density c_0 on the long timescale T,

$$\frac{\partial c_0}{\partial T} + d\overline{\boldsymbol{u}_{p_0}} \cdot \nabla c_0 = D_c \nabla^2 c_0 + \overline{g(n_0 = 1, c_0, \tau_s)} - \nu c_0. \tag{31}$$

Here, a bar denotes the period average of a function on the short timescale, so

$$\overline{\boldsymbol{u}_{p_0}} = \frac{1}{2\pi}\int_0^{2\pi} \boldsymbol{u}_{p_0}(\boldsymbol{x}, t)\, dt, \qquad \overline{g(n_0, c_0, \tau_s)} = \frac{1}{2\pi}\int_0^{2\pi} g(n_0 = 1, c_0, \tau_s)\, dt, \tag{32}$$

where $\boldsymbol{u}_{p_0} = \boldsymbol{u}_0/\phi$ is calculated using (23) with (17) and (27); and $g(n_0, c_0, \tau_s)$ is defined as in (28)–(30), with the pressure p calculated using (22). We solve this model subject to a specified initial seeding density, and no-flux conditions at the four scaffold boundaries. With total dimensionless cell flux defined as

$$\boldsymbol{J}_c = d\boldsymbol{u}_{p_0} c_0 - D_c \nabla c_0 \tag{33}$$

we therefore impose $\boldsymbol{J}_c \cdot \hat{\boldsymbol{n}} = 0$ at $x = 0, 1$, $y = 0, 1$, where $\hat{\boldsymbol{n}}$ denotes the outward normal to the scaffold boundary.

After prescribing an initial cell seeding density, we are able to solve for the pressure in the domain as described in Sect. 4, by first solving Eq. (19) subject to the stated boundary conditions ((20) and no-flux at $y = 0, 1$) via a finite volume method. We then calculate the fluid velocity using Eq. (23), following which a numerical integration is performed to obtain the average value $\overline{\boldsymbol{u}_{p_0}}$ over the short timescale. The same averaging procedure is used to calculate an average value for the cell proliferation term average, $\overline{g(n_0 = 1, c_0, \tau_s)}$ (note that this requires us to calculate the pressure p_0 using (22)). From this, we solve for the next time step of the cell density equation (31) using a simple Alternating Direction Implicit (ADI) method. This updated cell density is then used to determine permeability, pressure, and fluid velocity in the scaffold, at the next timestep, all of which are then in turn required for the next step in the cell density equation. This iterative process is continued until the user-defined final time is reached. The numerical codes used have been tested for convergence, and found to be first-order in space and time.

7 Results

We present sample numerical results from our model for a selection of different initial cell-seedings. For all initial seedings considered, the results are qualitatively similar for all loading or oscillatory flow scenarios, therefore we only show the dimensionless cell density evolution for a chosen loading scenario, followed by plots comparing total final cell yield for all loading protocols. To illustrate the evolution from the given initial condition, we show only results at dimensional times 240 and 600 hours (10 and 25 days, respectively), these being reasonable representative times for a tissue engineering experiment with loading (see, e.g., Wang et al. 2013). For all simulations described here, supplementary movie files showing dimensionless cell density evolution from start to finish are also available online.

7.1 Uniformly-Seeded Scaffold

We first consider the case most commonly aspired to in experiments: a uniform initial cell seeding. Figure 2 shows selected results from a simulation where a uniformly-

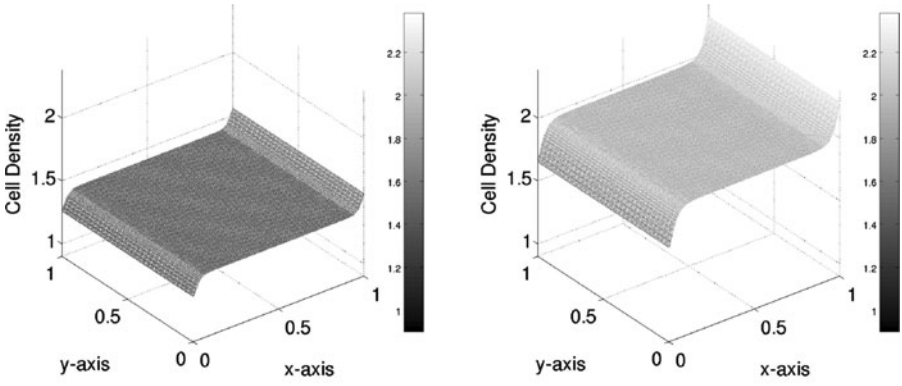

(a) $\Delta = 0.2$, $A = 0.5$, 240 hours (b) $\Delta = 0.2$, $A = 0.5$, 600 hours

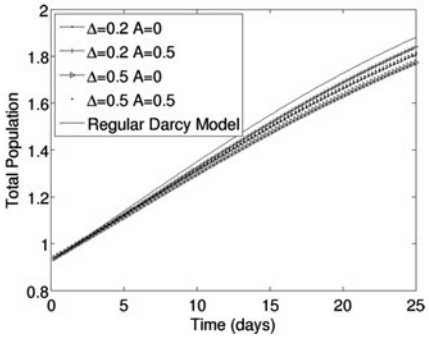

(c) Total cell populations

Fig. 2 (**a**), (**b**) Results for a uniform initial cell seeding with a chosen loading scenario (Δ, A-values). Dimensionless cell density is shown at different (dimensioned) times. (**c**) Comparison between alternative loading protocols

seeded scaffold is subjected to cyclic loading that induces a time variation in the permeability given by (17) (with $\Delta = 0.2$), and to an imposed flux with time-dependent oscillatory component given by (24) (with $A = 0.5$). (We may think of Δ as some measure of scaffold compression.) Figures 2a and 2b show snapshots of the dimensionless cell density after 240 and 600 hours (dimensional time) of perfusion plus loading, respectively; while Fig. 2c shows the total cell population as a function of time for several different loading/flow scenarios, characterized by changing parameters Δ and A. The case with no cyclic loading, where no cycle-averaging process is required, is referred to as "Regular Darcy Model" in this and subsequent figures.

Unsurprisingly, the evolution of the cell density profile in this case is not dramatic. The cell density evolves in a fairly uniform manner, but with lower densities towards the flow inlet ($x = 0$) and higher densities toward the outlet ($x = 1$). These "uptick/downtick" features are most easily seen in the surface plots shown in Fig. 3, where the cell densities at the final time are compared for all other loading protocols simulated. The evolution toward these final density profiles is given in the supple-

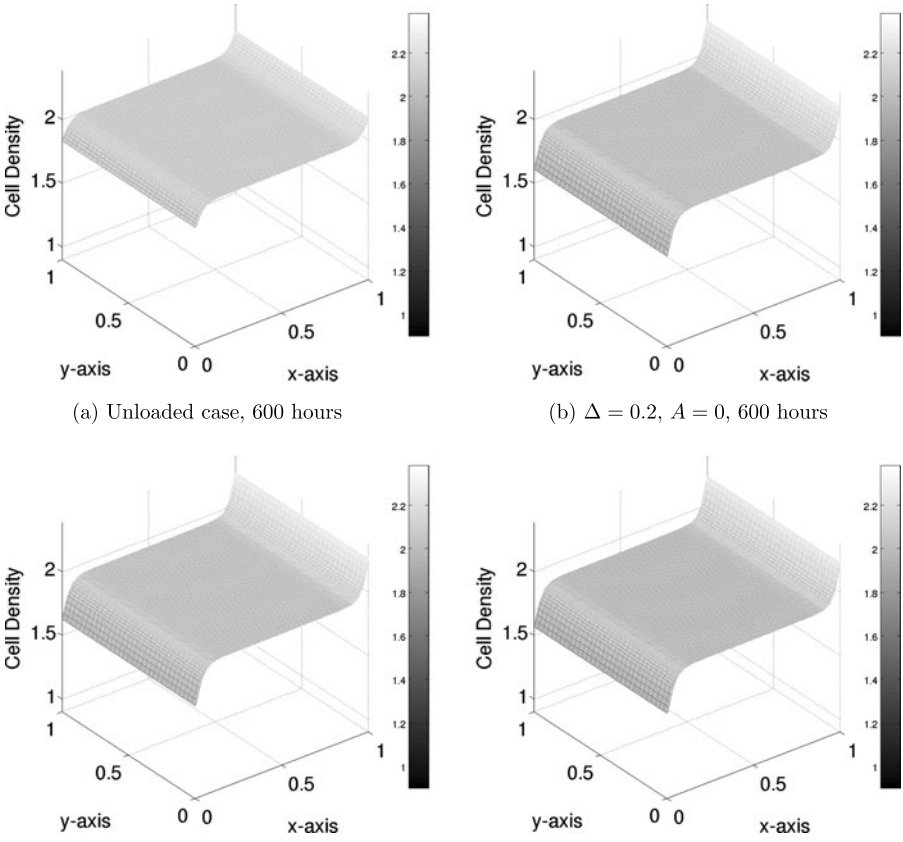

(a) Unloaded case, 600 hours

(b) $\Delta = 0.2$, $A = 0$, 600 hours

(c) $\Delta = 0.5$, $A = 0.5$, 600 hours

(d) $\Delta = 0.5$, $A = 0$, 600 hours

Fig. 3 Surface plots showing dimensionless cell density after 600 hours for a uniform cell seeding with different loading protocols

mental movie files that accompany the online version of the paper. The gradients near the inlet (downtick) and outlet (uptick) are present in all simulations, including those for the case without cyclic loading; but broadly speaking, the higher the degree of cyclic loading, the more pronounced these features are (this is demonstrated in Fig. 4d discussed further below; the up/downticks are much less pronounced in the unloaded case). They are probably largely attributable to the cellular advective drag, combined with our no flux condition on cells at the edges of the domain: given the net flow direction, this would certainly cause pile-up of cells at the outlet, and a dwindling of cell numbers near the inlet. That the features are not due simply to the net proliferation rate being higher or lower locally may be seen by plotting this function, $g(n_0 = 1, c_0, \tau_s) - \nu c_0$ (proliferation rate minus death rate; see (31)) for the scenario of Figs. 2a, b, as is done in Fig. 4. At the earlier time 240 hours, net proliferation is nearly uniform across the domain (Fig. 4a); while at the later time 600 hours, net proliferation is in fact highest at the inlet and lowest at the outlet (Fig. 4b); quite the reverse of what would be expected if net enhanced proliferation was responsible for

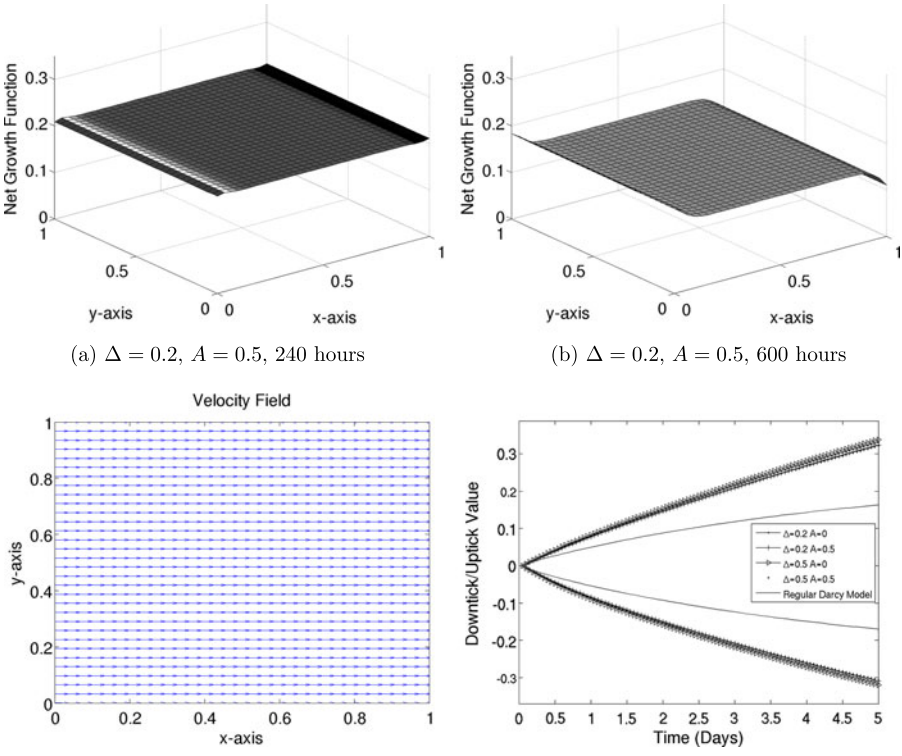

(a) $\Delta = 0.2$, $A = 0.5$, 240 hours

(b) $\Delta = 0.2$, $A = 0.5$, 600 hours

(c) $\Delta = 0.2$, $A = 0.5$, 600 hours

(d) Uptick/downtick feature height

Fig. 4 (**a**), (**b**) Net growth rate (growth minus death) for the uniform seeding scenario of Figs. 2a, b; (**c**) averaged velocity field within scaffold at time 600 hours (velocity at 240 hours is almost identical); (**d**) height of uptick (positive values)/downtick (negative values) features, relative to cell density at scaffold center, over time, for the different loading protocols considered in Fig. 3, showing clearly how these features are much less pronounced in the unloaded case

the observed features. The low value of the net proliferation function at the outlet at time 600 hours suggests that the cell population there is getting closer to the local carrying capacity, which suppresses further proliferation. Figure 4c shows the time-averaged velocity field across the scaffold at time 600 hours: this is nearly uniform, as we might expect (the velocity field at 240 hours is almost indistinguishable and is therefore not shown). Figure 4d shows how the size (height) of the up/downtick features at the scaffold's edge evolve over time for all loading scenarios tested: all loaded cases give rather similar results, while the unloaded case shows greatly suppressed growth of these features relative to the loaded cases. The width of these regions was also calculated and found to increase slowly in time, approximately linearly, but with very little difference between the various cases.

Figure 2c demonstrates that the final total cell population for all loading scenarios tested is in fact greatest for the unloaded (regular Darcy model) case under the given flow conditions, although the differences are not great. This could be due to a combination of factors: though shear stresses are higher under the compressive part of the cycle (leading, unless excessively high, to enhanced proliferation rates), they are lower under the "expansion" phase of the cycle, so the net effect may nearly cancel.

7.2 Peripherally-Seeded Scaffold

Achieving a uniform seeding right through to the center of the scaffold, as was assumed in the previous examples, can be experimentally challenging. It may be easier to seed the scaffold from its periphery, and rely on the migration of cells into the interior (under cellular diffusion and advection) to obtain the end result. Figures 5a, b show snapshots of a simulation where a linear decreasing gradient of cell density (into the scaffold in the direction normal to the wall) is imposed at each of the four scaffold walls, with a cell density that is maximum at the wall, dropping to zero a short distance into the scaffold interior. The seeded scaffold is subjected to cyclic loading that induces a time-dependent permeability given by (17), with $\Delta = 0.2$, and to an imposed flux with time-dependent oscillatory component given by (24), with $A = 0.5$.

Figure 5c shows a comparison of the results as the model loading/flow parameters Δ and A are varied. The total cell yield as a function of time is plotted for different combinations of Δ and A, and for the unloaded case (regular Darcy model). Only fairly modest differences are seen; for this particular seeding scenario the regular Darcy model again gives the best total cell yield. Figure 6 shows the final-time ($t = 600$ hours) cell density profiles for different loading scenarios. The corresponding movies showing the full evolution to these final states are provided as online supplementary material. The surface plots of Fig. 6 reveal that the final cell distributions for all loaded cases are very similar; but once again the unloaded case shows qualitative differences, particularly near the flow outlet.

As with the uniform seeding case considered in Sect. 7.1 we believe that the regions of enhanced and suppressed cell populations near the outlet and inlet are due to advective effects rather than to the net growth function values being higher or lower locally. Figures 7a, b show the net growth function (growth minus death terms from (31)) plotted for the scenarios of Figs. 5a, b, while Fig. 7c shows the averaged velocity field across the scaffold. As before, the net growth function acts against the

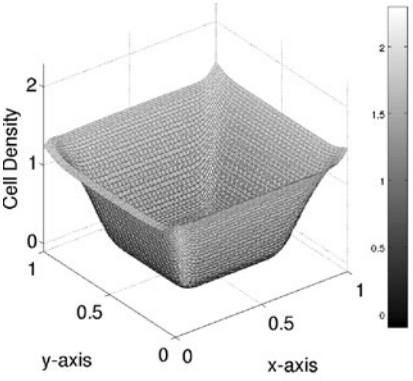

(a) $\Delta = 0.2$, $A = 0.5$, 240 hours

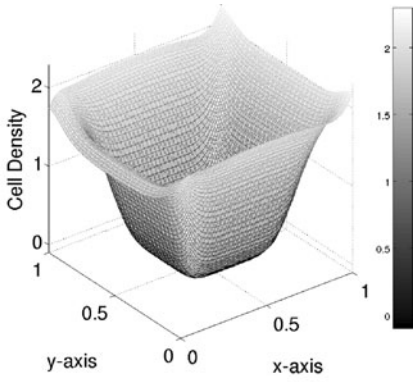

(b) $\Delta = 0.2$, $A = 0.5$, 600 hours

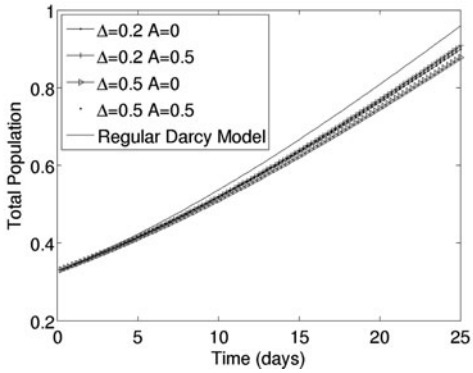

(c) Total cell populations

Fig. 5 (**a**), (**b**) Results for a peripheral cell seeding with a chosen loading scenario (Δ, A-values). Dimensionless cell density is shown at different (dimensioned) times. (**c**) Comparison between alternative loading protocols

observed trend of enhanced cell population at the outlet and suppressed population at the inlet: bearing in mind the no-flux conditions on cells at inlet and outlet, one can see from Fig. 7 how the net growth function and cellular advection combine to give the cell distributions observed in Figs. 5a, b.

7.3 Centrally-Seeded Scaffold

As a final comparison, we consider a scaffold seeded only at its center. Figure 8 shows snapshots of the cell density evolution over time for the same parameters considered previously, together with the comparison plot showing the total cell yield over time for the different loading scenarios. Once more the unloaded model wins out in terms of the final cell yield, all other loading scenarios giving very similar, slightly lower, yields. For this case, the final cell density surface plots are all qualitatively very similar: as we saw in the previous examples, the main differences in cell density appear at the edges of the scaffold, and here all cell densities remain relatively low at the edges, even after 600 hours. Hence, we do not show the final surface plots for all

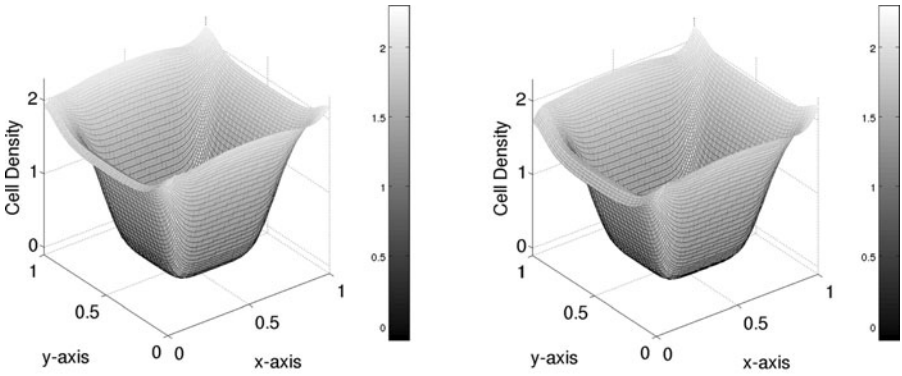

(a) Unloaded case, 600 hours

(b) $\Delta = 0.2$, $A = 0$, 600 hours

(c) $\Delta = 0.5$, $A = 0.5$, 600 hours

(d) $\Delta = 0.5$, $A = 0$, 600 hours

Fig. 6 Surface plots of dimensionless cell density after 600 hours for peripheral cell seeding with different loading protocols

cases with this initial seeding scenario. In Fig. 9, we show the net growth functions (growth minus death terms in Eq. (31)) corresponding to Figs. 8a, b, together with the velocity field throughout the scaffold at time 600 hours. Figure 9b shows that at late times the net growth in the central region where the cell population is highest is (while still large) beginning to be suppressed, as the population starts to approach the carrying capacity locally.

8 Extensions to the Model

The basic model presented for our perfusion bioreactor is a good starting-point for a macroscale description of osteocytes or chondrocytes within a porous scaffold under nutrient perfusion. Moreover, it can be used to predict cell proliferation over relevant timescales for both steady perfusion, and oscillatory perfusion with cyclic compression, by exploiting the two-timescale analysis and period-averaging as described above. As noted in the Introduction, many of the differences observed under

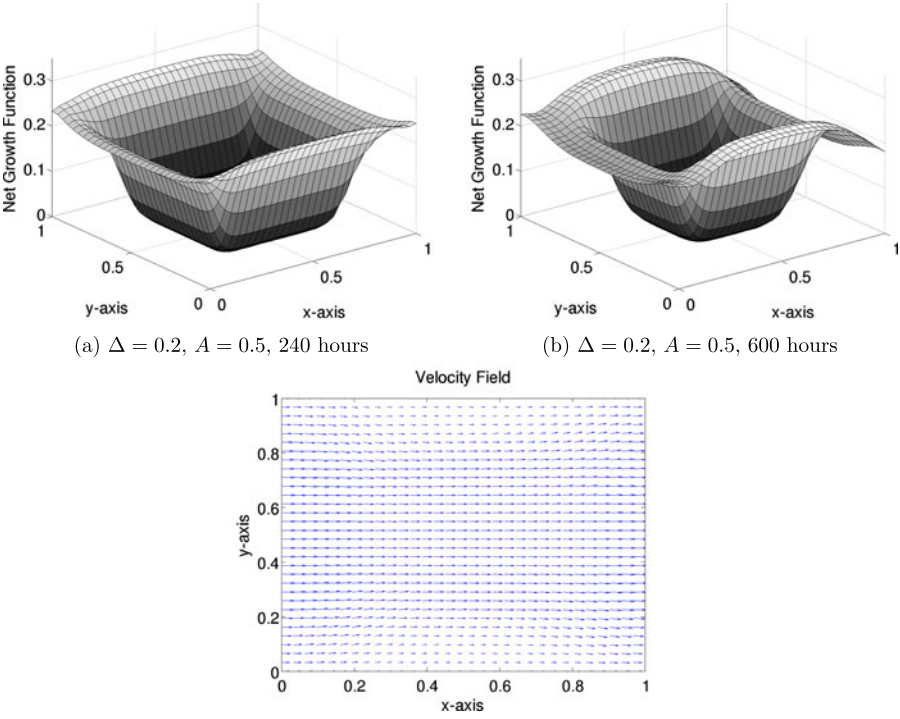

(a) $\Delta = 0.2$, $A = 0.5$, 240 hours

(b) $\Delta = 0.2$, $A = 0.5$, 600 hours

(c) $\Delta = 0.2$, $A = 0.5$, 600 hours

Fig. 7 (**a**), (**b**) Net growth rate (growth minus death) for the scenario of Figs. 5a, b; (**c**) averaged velocity field within scaffold at time 600 hours (velocity at 240 hours is almost identical)

loading (compared with no loading) concern aspects such as stem-cell fate (differentiation into different cell types), something our model presently says nothing about. Regarding the effect of cyclic loading on proliferation, the evidence is not altogether conclusive: While the majority of studies seem to agree that oscillatory *flow* does not lead to enhanced proliferation (McCoy and O'Brien 2010), cyclic *compression* may (El Haj and Cartmell 2010).

These observations suggest that a model capable of distinguishing the loaded and unloaded cases should explicitly incorporate some additional biology. Here, we briefly outline some possible directions for future models (but provide no simulations for these possible model extensions).

Desensitization Under Steady Shear One hypothesis is that a constant biomechanical stimulus leads to cellular desensitization—the continued uniform application of stress or strain results in tolerance of the conditions by the cell, turning off the (possibly beneficial) response (see McCoy and O'Brien 2010 and references therein). In our model, the pulsatile nature of the loading is represented by two parameters: Δ, which is dimensionless and may be thought of as a measure of scaffold strain; and A, the amplitude of any flow oscillation (relative to the underlying steady flow). The simplest way to incorporate the desensitization into the existing model is to modify the

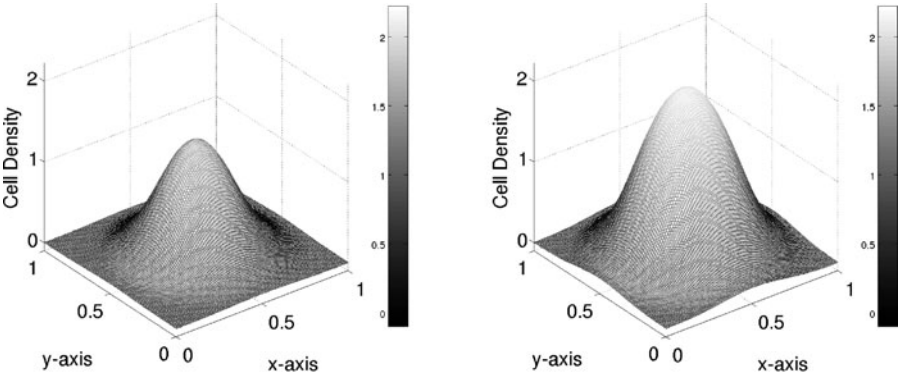

(a) $\Delta = 0.2$, $A = 0.5$, 240 hours (b) $\Delta = 0.2$, $A = 0.5$, 600 hours

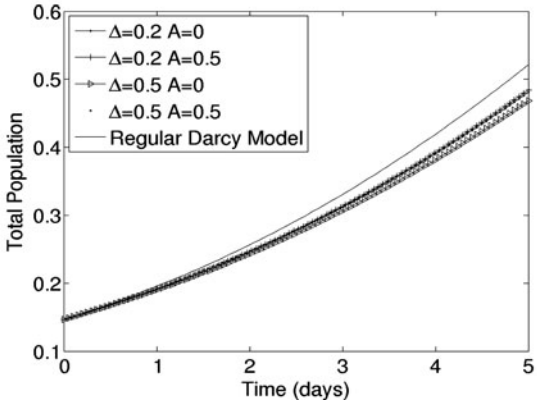

(c) Total cell populations

Fig. 8 Results for a central cell seeding with a chosen loading scenario, and comparison between this and alternative loading protocols

proliferation function $g(n, c, \tau_s)$ (see (28)) so that in the unloaded (or suboptimally loaded) case it decays over the long timescale of proliferation to some lower value. Since data suggest that only compressive loading affects proliferation to any extent, we propose in the first instance a modification that depends only on Δ. For example, if one assumes that there is some "optimal" value of Δ, Δ_{opt} say, then premultiplying $g(n, c, \tau_s)$ in (28) by

$$f(T) = 1 - \beta|\Delta_{\text{opt}} - \Delta|\left(1 - e^{-\ell T}\right), \quad \beta, \ell > 0,$$

would have the desired effect, at least for moderate loading scenarios. Thus, in the optimally-loaded case $\Delta = \Delta_{\text{opt}}$, $f(T) \equiv 1$ and there is no diminution in proliferation; but in the unloaded case $\Delta = 0$, $f(T) = 1 - \beta\Delta_{\text{opt}}(1 - \exp(-\ell T))$, and over dimensionless times greater than $1/\ell$ (on the long timescale) the proliferation rate drops by a factor $(1 - \beta\Delta_{\text{opt}})$. Cases of intermediate compression, $0 < \Delta < \Delta_{\text{opt}}$ lead to smaller decreases in the proliferation rate. Note that with this simple model excessive compression is also detrimental; a compression of $\Delta = 2\Delta_{\text{opt}}$ is as bad as

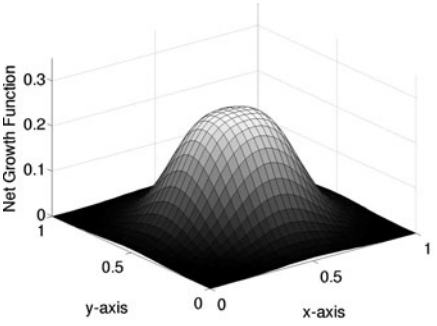

(a) $\Delta = 0.2$, $A = 0.5$, 240 hours

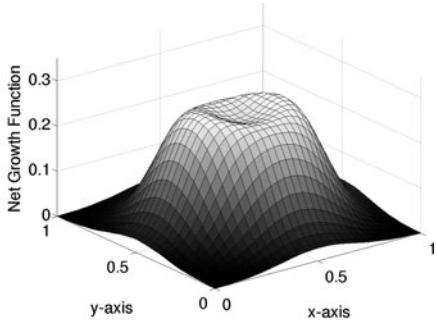

(b) $\Delta = 0.2$, $A = 0.5$, 600 hours

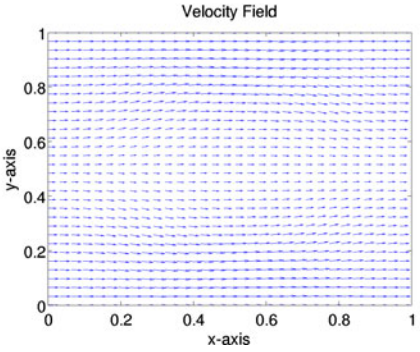

(c) $\Delta = 0.2$, $A = 0.5$, 600 hours

Fig. 9 (**a**), (**b**) Net growth rate (growth minus death) for the scenario of Figs. 8a, b; (**c**) averaged velocity field within scaffold at time 600 hours (velocity at 240 hours is almost identical)

no loading. Though this model takes no explicit account of the dependence on the loading frequency ω^*, one could build this in by making the parameters β, ℓ, Δ_{opt} depend on the loading frequency.

Release of Biochemical Stimuli Under Loading It is known that cells release various biochemical signals in larger quantities under periodic loading than they would under conditions of constant shear. One could model the release of one or more such stimuli (at concentration e) by an equation of the kind

$$\frac{de}{dT} = \gamma \Delta \left(c - \frac{e}{\hat{e}} \right), \quad \gamma, \hat{e} > 0,$$

where it is understood that, in the spirit of the averaging carried out in Sect. 4.1, we consider the leading-order concentration of e on the long timescale. Here, $\hat{e}$ represents a maximal production of generic signal per cell (likely dependent on Δ). In this model, production of signal e is suppressed when there is no loading ($\Delta = 0$).

Given sufficient experimental data on the specific effects of biochemical signal e, one could then incorporate e-dependence into the growth-rate and/or death rates in the cell-proliferation equation.

Modeling release of specific biochemical species in this way also allows for the possibility of extending our model to account for cellular differentiation. In the simplest case, one could start with a population of stem cells, which may release two different genetic markers e_1 and e_2, depending on the loading conditions. One could then use the local concentrations of e_1 and e_2 to determine the cell fate at that location. Such a model would allow us to track the populations of different cell types within the scaffold. Again, however, more experimental data is needed to propose a convincing model of this kind.

9 Discussion

We have presented a minimal model for the proliferation of cells (e.g., chondrocytes) under cyclic loading and periodic pulsatile flow. Since the loading occurs on a timescale very much shorter than that of cellular proliferation, a two-timescale analysis together with period-averaging is exploited to derive a closed-form model for the evolution of cell density over the long timescale of proliferation. The model is very simple in that the effect of the loading is captured only by its effect on the fluid dynamics and hence the shear stress, which affects the local proliferation rate. Other than the brief discussion in Sect. 8 above, no attempt is made to model other mechanotransductive effects due to the loading, such as up-regulation of cellular genetic markers, which may impact the long-term proliferation and functionality of the tissue. Our model therefore investigates the hypothesis that differences in final outcomes under loading could be due mainly to the altered fluid dynamics and shear stresses, assuming that these impact proliferation in the same way as in an "unloaded" model.

The model was simulated for several different loading scenarios, and compared to results with no loading, for a selection of different initial cell seedings. Though the final pattern of cells within the scaffold shows qualitative differences in loaded versus unloaded cases, the final cell yields show only modest differences. In all the cases presented here, the highest total yield was (marginally) attained with the unloaded case; however, in some of our simulations (not reproduced here) with different initial seedings the loaded cases outperformed the unloaded case, again marginally. We emphasize that our model can say nothing about functionality of the final tissue in different cases. That said, there are some clear differences between loaded and unloaded cases, which may be seen in Figs. 3 and 6 (and in the accompanying movie files online). While all loading scenarios lead to very similar final outcomes, the cell distribution in the unloaded case differs noticeably at the flow outlet $x = 1$, the cell density there being consistently lower than in any comparable loaded case. We attribute this feature primarily to the effects of cellular advection near the boundaries.

Given the large parameter space, even for the simple model presented here, we have not yet fully explored all aspects of our model. In particular, we cannot state with certainty whether all reasonable model inputs will generate reasonable outputs (or conversely, whether unreasonable inputs may generate reasonable outputs). Nonetheless, our findings, when considered alongside experimental evidence demonstrating that loading can lead to profound differences in the final outcomes (e.g., Buschmann

et al. 1995), strongly suggest that in fact the effects of loading are deeper than this model can capture, and that specific account must be taken of additional cell biology. We believe, however, that our model provides a robust starting-point for a more sophisticated model that takes explicit account of additional mechanotransductive effects (hence our discussion in Sect. 8).

An important assumption that enabled our period-averaged model to be derived explicitly was that the construct is well nourished throughout. While this may be an ideal situation, the cost of the culture medium means that it may not be economically feasible to supply it in excess. Further work is needed to study the more complicated model that results when nutrient levels vary appreciably throughout the scaffold. This situation was considered for the simpler cases of static culture (Lewis et al. 2005) and steady perfusion (Shakeel et al. 2013; Pohlmeyer et al. 2013). Such models can provide useful predictions of conditions under which nutrient depletion zones may form, with negative consequences for the growing cells. We plan to extend our modeling to such scenarios in the near future.

Acknowledgements Both authors acknowledge partial financial support from KAUST under Award No. KUK-C1-013-04 in the form of OCCAM Visiting Fellowships. We thank Drs Treena Arinzeh, Shahriar Afkhami, Michael Siegel (NJIT), and Sarah Waters (Oxford) for useful guidance with the development and numerical solution of the model.

References

Babalola, O. M., & Bonassar, L. J. (2009). Parametric finite element analysis of physical stimuli resulting from mechanical stimulation of tissue engineered cartilage. *J. Biomech. Eng.*, *131*(6), 061014.

Buschmann, M. D., Gluzband, Y. A., Grodzinsky, A. J., & Hunziker, E. B. (1995). Mechanical compression modulates matrix biosynthesis in chondrocyte/agarose culture. *J. Cell Sci.*, *108*(4), 1497–1508.

Chung, C., Chen, C., Chen, C., & Tseng, C. (2007). Enhancement of cell growth in tissue-engineering constructs under direct perfusion: modeling and simulation. *Biotechnol. Bioeng.*, *97*, 1603–1616.

Chung, C., Chen, C., Lin, T., & Tseng, C. (2008). A compact computational model for cell construct development in perfusion culture. *Biotechnol. Bioeng.*, *99*, 1535–1541.

Coletti, F., Macchietto, S., & Elvassore, N. (2006). Mathematical modeling of three-dimensional cell cultures in perfusion bioreactors. *Ind. Eng. Chem. Res.*, *45*, 8158–8169.

Curtis, A., & Riehle, M. (2001). Tissue engineering: the biophysical background. *Phys. Med. Biol.*, *46*, 47–65.

El Haj, A., & Cartmell, S. (2010). Bioreactors for bone tissue engineering. *J. Eng. Med.*, *224*, 1523–1532.

El Haj, A., Minter, S., Rawlinson, S., Suswillo, R., & Lanyon, L. (1990). Cellular responses to mechanical loading in vitro. *J. Bone Miner. Res.*, *5*(9), 923–932.

Lappa, M. (2003). Organic tissues in rotating bioreactors: fluid-mechanical aspects, dynamic growth models, and morphological evolution. *Biotechnol. Bioeng.*, *84*(5), 518–532.

Lewis, M., MacArthur, B., Malda, J., Pettet, G., & Please, C. (2005). Heterogeneous proliferation within engineered cartilaginous tissue: the role of oxygen tension. *Biotechnol. Bioeng.*, *91*, 607–615.

Lutianov, M., Shialesh, N., Roberts, S., & Kuiper, J.-H. (2011). A mathematical model of cartilage regeneration after cell therapy. *J. Theor. Biol.*, *289*, 136–150.

Malda, J., Rouwkema, J., Martens, D., Le Comte, E., Kooy, F., Tramper, J., van Blitterswijk, C., & Riesle, J. (2004). Oxygen gradients in tissue-engineered pegt/pbt cartilaginous constructs: measurement and modelling. *Biotechnol. Bioeng.*, *86*(1), 9–18.

Mauck, R. L., Soltz, M. A., Wang, C. C. B., Wong, D. D., Chao, P.-H. G., Valhmu, W. B., Hung, C. T., & Ateshian, G. A. (2000). Functional tissue engineering of articular cartilage through dynamic loading of chondrocyte seeded agarose gels. *J. Biomech. Eng.*, *122*(3), 252–260.

McCoy, R., & O'Brien, F. (2010). Influence of shear stress in perfusion bioreactor cultures for the development of three-dimensional bone tissue constructs: a review. *Tissue Eng., Part B*, *16*(6), 587–601.

Moo, E. K., Herzog, W., Han, S. K., Abu Osman, N. A., Pingguan-Murphy, B., & Federico, S. (2012). Mechanical behaviour of in-situ chondrocytes subjected to different loading rates: a finite element study. *Biomech. Model. Mechanobiol.*, *11*(7), 983–993.

Obradovic, B., Meldon, J. H., Freed, L. E., & Vunjak-Novakovic, G. (2000). Glycosaminoglycan deposition in engineered cartilage: experiments and mathematical model. *AIChE J.*, *46*, 1860–1871.

O'Dea, R., Waters, S., & Byrne, H. (2008). A two-fluid model for tissue growth within a dynamic flow environment. *Eur. J. Appl. Math.*, *19*(6), 607–634.

O'Dea, R., Waters, S., & Byrne, H. (2009). A multiphase model for tissue construct growth in a perfusion bioreactor. *Math. Med. Biol.*, *27*(2), 95–127.

Osborne, J., O'Dea, R., Whiteley, J., Byrne, H., & Waters, S. (2010). The influence of bioreactor geometry and the mechanical environment on engineered tissues. *Journal of Biomechanical Engineering*, *132*(5), 051006.

Pohlmeyer, J., Waters, S., & Cummings, L. J. (2013). Mathematical model of a growth factor driven haptotaxis and proliferation in a tissue engineering scaffold. *Bull. Math. Biol.*, *75*(3), 393–427.

Porter, B., Zauel, R., Stockman, H., Guldberg, R., & Fyhrie, D. (2005). 3-D computational modelling of media flow through scaffolds in a perfusion bioreactor. *J. Biomech. Eng.*, *38*(3), 543–549.

Raimondi, M., Boschetti, F., Falcone, L., Migliavacca, F., Remuzzi, A., & Dubini, G. (2004). The effect of media perfusion on three-dimensional cultures of human chondrocytes: integration of experimental and computational approaches. *Biorheology*, *41*(3), 401–410.

Schätti, O., Grad, S., Goldhahn, J., Salzmann, G., Li, Z., Alini, M., & Stoddart, M. J. (2011). A combination of shear and dynamic compression leads to mechanically induced chondrogenesis of human mesenchymal stem cells. *Eur. Cells Mater.*, *22*, 214–225.

Sengers, B., Taylor, M., Please, C., & Oreffo, R. (2007). Computational modelling of cell spreading and tissue regeneration in porous scaffolds. *Biomaterials*, *28*, 1926–1940.

Shakeel, M., Matthews, P., Waters, S., & Graham, R. (2013). A continuum model of cell proliferation and nutrient transport in a perfusion bioreactor. *Math. Med. Biol.*, *30*(1), 21–44.

Wang, N., Grad, S., Stoddart, M. J., Niemeyer, P., Sudkamp, N. P., Pestka, J., Alini, M., Chen, J., & Salzmann, G. M. (2013). Bioreactor-induced chondrocyte maturation is dependent on cell passage and onset of loading. *Cartilage*, *4*(2), 165–176.

Zhou, S., Cui, Z., & Urban, J. (2004). Factors influencing the oxygen concentration gradient from the synovial surface of articular cartilage to the cartilage-bone interface: a modeling study. *Arthritis Rheum.*, *50*(12), 3915–3924.